Energy & Buildings 205 (2019) 109532

Contents lists available at ScienceDirect

Energy & Buildings

journal homepage: www.elsevier.com/locate/enbuild

Heat transfer and condensation in an earth-air heat exchanger: 2D/3D numerical modeling validated by experimental measurements

Geoffroy Chardome*, Véronique Feldheim

UMONS – Faculté Polytechnique – Service Thermique et Combustion, Rue de l'Épargne, 56 – 7000 Mons – Belgique

ARTICLE INFO

Article history:
Received 1 February 2019
Revised 26 September 2019
Accepted 14 October 2019
Available online 16 October 2019

ABSTRACT

The earth-air heat exchanger (EAHE) or "Puits canadien" in French consists of buried pipes for the hygienic ventilation of a building. This allows a preheating of the ventilation air in winter and a passive cooling in summer. This technique uses the thermal capacity of the earth to buffer and phase out the periodic variation of the outside temperature. Various numerical models, validated by experimental measurements, have been made to simulate heat transfer and condensation over a period of one year. To resolve the unsteady 3D configuration of the problem, a pseudo 3D model was used to determine the temperature field. As the circulating air also carries moisture, a phenomenon of condensation will take place, creating a particular biotope that can contaminate the hygienic air by the biocenosis. The first part of the study is the condensate evaluation. It will be supplemented in a second step by a metagenomic study of biocenosis.

1. Introduction

As the soil can be assimilated to a semi-infinite homogeneous medium, the periodic variation of its temperature is damped and out of phase with the variation of the temperature of the surface temperature [1–4]. To benefit from this damping and phase shift, the air required for the hygienic ventilation of a building passes through one or more pipes buried in the ground, making it possible to reduce the consumption of a building both during the winter period and summer. This technique is part of passive air conditioning systems [5].

This principle of ventilation is very old, it was already used by Iranian architects in 3000 BCE who used underground tunnels and wind tower or "catch-wind" for the cooling and heating of buildings [6–8].

The aim of this study is to create a numerical model for the simulation of an earth-air heat exchanger (EAHE) to quantify the condensates produced during certain periods of the year. Indeed, stagnant condensates in an earth-air heat exchanger can be at the origin of the development of molds and bacteria representing a health risk that it is necessary to study, although the presence of filters at the level of the ventilation system seems to be a sufficient measure to avoid this health risk, as demonstrated in the studies [9] and [10].

We propose a predictive study on the formation of condensates within the heat exchanger, for which we developed a pseudo 3D model using the COMSOL Multiphysics software and a MATLAB interface. The model allows to evaluate the quantity of condensates in the EAHE and its temperature, at any given time step.

First, in order to validate the pseudo 3D model, the condensation phenomenon will be neglected, which has no significant impact on heat transfer. The results obtained will be compared to 3D models as well as data collected on an existing installation monitored continuously.

The simulations are carried out for a complete year with a time step limited of one hour to be able to study the effects of the exchanger on the periodic annual or daily variation of the temperatures.

2. Brief state of the art

The indoor air quality in buildings is particularly studied given the impacts on the health and productivity of the occupants [11,12]. The objective is to reduce the ventilation rates to limit the energy consumption of the buildings while guaranteeing the air quality. To characterize the air quality in buildings, we find essentially studies on physical and chemical pollutants [8,13,14]. The pollution by biological agents is not generally used to characterize the air quality, it will be the subject of a study complementary to this one. The health risk associated with the development of microorganisms in EAHE has already been studied [15]. The health risk exists but is limited, a difference between bacteria and mould

* Corresponding author.
E-mail address: geoffroy.chardome@umons.ac.be (G. Chardome).

https://doi.org/10.1016/j.enbuild.2019.109532
0378-7788/

Nomenclature

a	thermal diffusivity, $m^2.s^{-1}$
c	specific heat capacity, $J.kg^{-1}.K^{-1}$
c_a	specific heat capacity of dry air, $J.kg^{-1}.K^{-1}$
c_H	specific heat capacity of moist air, $J.kg^{-1}.K^{-1}$
c_v	specific heat capacity of water vapor, $J.kg^{-1}.K^{-1}$
e_a	average absolute error on temperature, K
e_{max}	maximum error on temperature, K
f	friction factor
$h_{surface}$	convective heat transfer coefficient at the interface between the ground and the external environment, $W.m^{-2}.K^{-1}$
h_{tube}	convective heat transfer coefficient at the inner surface of the pipe, $W.m^{-2}.K^{-1}$
i_{air}	air specific enthalpy, $J.kg^{-1}_{dry\ air}$
i_{sat}	specific enthalpy of the air at saturation for the temperature of the inner surface of the pipe, $J.kg^{-1}_{dry\ air}$
k	thermal conductivity, $W.m^{-1}.K^{-1}$
K_D	diffusion coefficient of material, $kg.s^{-1}.m^{-2}$
L_c	latent heat of condensation, $J.kg^{-1}$
$\dot{m}_{air}$	air mass flow, $kg.s^{-1}$
$\dot{m}_{cond}$	condensates mass flow, $kg.s^{-1}$
M	mass flux, $kg.s^{-1}.m^{-2}$
$\vec{n}$	unit normal vector
Nu	Nusselt number
Pr	Prandtl number
q_0	latent heat flux at the inner surface of the pipe, $W.m^{-2}$
q_{solar}	solar heat flux, $W.m^{-2}$
q_{tot}	total heat flux at the inner surface of the pipe, $W.m^{-2}$
Q_{conv}	convective heat flow, W
Q_{lat}	latent heat flow, W
Q_{tot}	total heat flow, W
Re	Reynolds number
$S_{section}$	heat transfer surface for the considered section, m^2
T	temperature, °C
T_{ext}	outside temperature, °C
T_{air}	air temperature, °C
T_{env}	environment temperature, °C
T_{wall}	temperature of the inner surface of the pipe, °C
$\vec{\nabla}T$	gradient of temperature, $K.m^{-1}$
v_{wind}	wind velocity, $m.s^{-1}$
x	humidity ratio, $kg_{water}.kg^{-1}_{dry\ air}$
x_{sat}	saturation humidity ratio, $kg_{water}.kg^{-1}_{dry\ air}$
Y_{air}	vapor mass title of the air, $kg_{vapor}.kg^{-1}_{mixed}$
Y_{sat}	vapor mass title of the air at saturation for the temperature of the inner surface of the pipe, $kg_{vapor}.kg^{-1}_{mixed}$

Greek symbols

ε	emissivity
ρ	density, $kg.m^{-3}$
σ	Stefan–Boltzmann constant, $5{,}67.10^{-8}\ W.m^{-2}.K^{-4}$

Subscripts

in	the inlet of the considered section
out	the outlet of the considered section
wall	of the pipe wall
wall,m	average of the pipe wall

has been made. The material used for the pipes has no impact, but the filters must be given special attention and the EAHE regularly cleaned.

The EAHE technique has been studied all over the world and some articles make the state of the art on the research in this field, essentially on the thermal aspects related to this technique.

- A special analysis on the coupling of EAHE to a mechanical ventilation system was done in [16]. The conclusion of this study is that an EAHE can be installed in different types of climate and be designed both for cool climates (e.g. Germany) and for warmer countries (e.g. India). Many types of buildings combine ventilation systems with EAHE and if the thermal conception is good and the EAHA is coupled with other low-energy cooling techniques (e.g. night cooling), an air-conditioning system is not necessary.
- The performance of an EAHE depends on the earth surface conditions and can be improved significantly by appropriate modification on the earth surface [17]. In a cold climate, by blackening and glazing the earth surface and in a hot and dry climate, by shading and wetting the earth surface.
- A study that defines general climate independent design guidelines for daily or annual temperature damping based on air flow has been reported by Hollmuller et al. [18]. The lack of interest in preheating ventilation air when the EAHE is coupled with a heat recovery unit has also been proven. An analysis of the occurrence of condensation in the EAHE for a central European climate showed that the risk is insignificant for a shallow and compact configuration (daily damping) but present for a deep and distant pipe configuration (annual damping).
- Soni et al. [19] have focused their work on the ground coupled heat exchanger (GCHE) and specially on performance of both types of GCHE systems namely: earth–air heat exchanger (EAHE) and ground source heat pump (GSHP) systems. The payback period for EAHE is small but the energy saving is more important for GSHP. The EAHE systems technology is well established whereas GSHP systems technology needs to be accepted in developing countries. However, they would make it possible to limit energy consumption and therefore the construction of production systems.
- Various experimental and analytical studies have described in detail [20,21] the effects of geometry, airflows and soil characteristics on the performance of EAHE [22]. The inlet temperature and flow velocity of the air have a significant effect on the thermal performance of EAHE system. The knowledge of soil thermo-physical properties is crucial, but the pipe material has a minimal effect on the overall heat transfer between air and soil. It is recommended to use multiple pipes of small diameter instead of single pipe with a large diameter but while using multiple pipes, the spacing between pipes becomes a critical parameter when EAHE is put under operation continuously for longer durations in harsh ambient conditions. To reduce the installation's costs the distance between the pipes should be reduced gradually along the length of pipe because heat transfer rate at the upstream section of pipe is higher than that at downstream section. A depth of EAHE pipe greater than 3–4 m does not bring any improvement compared to a classical depth of about 2 m because the ground temperature varies little beyond this and the duration of operation of EAHE system should be managed aptly in such a manner that the ground recovers its thermal properties.
- An analysis of research in the field in Turkey [6] and in India [23] shows the utility of EAHE system to save energy by preheating and precooling air for the air conditioning of buildings and to reduce power consumption, CFC and HCFC consumption and greenhouse gas emissions. For the moment United States

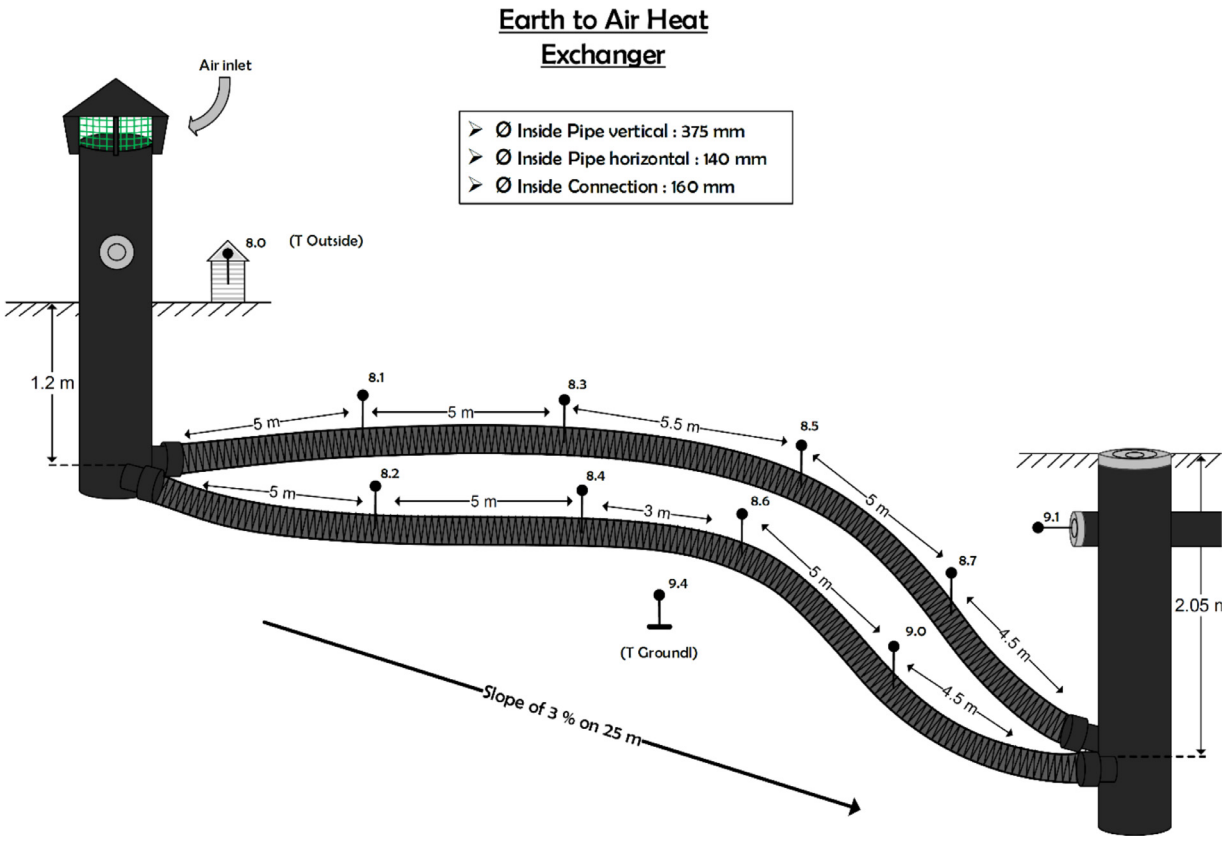

Fig. 1. Scheme of the monitored installation and location of the thermocouples.

and Europe are world leaders in the use of EAHE systems but the development potential is present all over the world.

3. Experimental setup and results

3.1. Installation analyzed

The installation is located on the site of the Technical Campus of the "Haute École en Hainaut" (HEH) in Mons, Belgium. Its scheme is given on Fig. 1.

The EAHE is made of HDPE (High Density Polyethylene) and consists of a suction element associated with a vertical shaft with a diameter of 375 mm which sinks into the ground to a depth of 1.25 m. It is then divided into two pipes each of 25 m's length having an inside diameter of 140 mm and forming an angle to ensure a distance of 1 m between them and thus to prevent one pipe from influencing the temperature of the soil around the second pipe. A slope of 3% ensures the evacuation of the condensates.

Given the EAHE layout, approximately halfway along their horizontal course, the pipes make a 90° horizontal angle. At the end of their horizontal course they join again in a vertical shaft of 375 mm diameter and 2 m depth and in which the condensates accumulate. Two to three times a year, the condensates are removed using an empty cellar pump installed for this purpose. Unfortunately, in 2015, there has been no monitoring system to measure the condensate quantities discharged. Once the air comes out of this vertical shaft, it enters the building's crawl space through a fully insulated pipe (to reduce the heat losses) and is then sucked by a controlled mechanical ventilation system with heat recovery, which pulses this air in a control room.

It should be noted that the depth of the installation is not optimal. The EAHE is expected to have an average depth of about 2.25 m, while the installation was conducted at an average depth of 1.625 m. The soil temperature therefore varies more during the year and the potential for cooling in summer and preheating in winter is reduced. It is the presence of the water table that has imposed the limitation of the depth of the EAHE, because although the water and the radon tightness of this one is ensured by heat-shrink sleeves, it was technically difficult to dig below the level of the water table. The presence of the latter nevertheless has a positive effect, as it promotes the exchanges between the EAHE and the soil.

The fan speed is kept constant throughout the year, the pressure drops of the installation varying little, the air flow rate will be considered constant. The measured value is 250 $m^3.h^{-1}$.

3.2. Measurement system

The installation is equipped with waterproof and shielded thermocouples to prevent any measurement error due to the condensation on the thermocouple. They are of type "T" 6 × 150 mm stainless steel sheath with waterproof terminal block and PVC head. The connection is made of type "M20" and is done by adapted PVC cable gland. The compensation cable is also made of type "T" 2 × 1.34 mm^2 PVC insulated with internal foaming foil of aluminum. It is possible to measure the temperature of the ground, of the outside air, in different places of the EAHE and obviously at the exit of the EAHE itself.

A thermocouple of type "T" is composed of copper and constantan (copper and nickel alloy). Its accuracy is very important, and the standard error is of the order of 0.1 °C.

The air flow rate is measured twice a month at the supply air grille with a funnel and an anemometer.

Table 1
Physical characteristics of the soil.

	c	ρ	k	a	ε
	$J.kg^{-1}.K^{-1}$	$kg.m^{-3}$	$W.m^{-1}.K^{-1}$	$m^2.s^{-1}$	
Soil	1000	1800	0.58	3222.10^{-7}	0.95

3.3. Type of soil studied

Given the completion of a geotechnical campaign, due to the works related to the pipeline of a nearby river, the depth of the water table (2.5 m) and the soil composition at the EAHE level are known [24]. It is composed of a brown sandy-stony backfill, whose characteristics are given in Table 1. The density was measured during the geotechnical campaign, the other characteristics were chosen according to the nature of the soil [25]. A sensitive study on heat capacity and thermal conductivity will be presented in point 5.3.

3.4. Experimental results

Every 15 min, the measuring system records the outside temperature, the soil temperature at 2 m depth, the temperatures in each pipe every 5 m and the temperature at the output of the EAHE. To limit the simulation data, an average of the measurements has been made to get hourly values. The probe measuring the ground temperature is located between the pipes but deeper. The distance between the probe and the pipes is 70 cm, the result of the measurement is therefore impacted by the presence of the pipes. Normally, the annual average of the outside temperature (12.4 °C) and soil temperatures (14.6 °C) should be the same.

The EAHE is monitored since June 2014. For this article the reference year is the year 2015 because it's the first full year. In order to limit the impact of the choice of the initial values in the numerical models, the readings start on 01 December 2014 at 01:00 am, which corresponds to the time - 743. January 01, 2015 at 00: 00 h is taken as a reference at 0 o'clock and January 01, 2016 at 00: 00 o'clock corresponds to the time 8760.

3.5. Flow and velocity of the air within the EAHE

Since the installation is actually composed by two pipes, it is interesting to observe the evolution of the temperature inside each tube. For that, we compared the temperatures at the probes 8.3 and 8.4, both placed at a distance of 11.20 m from the EAHE inlet and illustrated in Fig. 1.

Fig. 3 shows that the temperatures given by these two probes are very close and it can be concluded that the phenomena (in particular the heat transfers) are identical within each pipe. The air velocity inside the pipes being the only unknown influencing the heat transfer, it must have a fairly close value in both pipes, and we can say that the flow is evenly distributed inside the pipes.

The total measured air flow circulating in the EAHE is 250 $m^3.h^{-1}$, so we consider that an air flow of 125 $m^3.h^{-1}$ circulates inside each pipe.

4. EAHE models

4.1. EAHE's models in the literature

The modelling of EAHE has already been the subject of many studies. Their goals can be variable. It can be a question of validating the results obtained using a simplified analytical model by comparing them with the results obtained using a numerical model or validating a model, whether analytical or numerical, by comparing the results of simulations with experimental values.

The modelling of heat transfers in the soil matrix is complex which explains the number of studies on the subject. Given the heterogeneous nature of the soil matrix, it is necessary to make simplifying assumptions because of the difficulty of obtaining an exact analysis of the composition of the soil matrix and the number of physical phenomena taking place in the system.

There are different kinds of models. The most simplified studies use a 1D model by considering the temperature of the soil matrix as a fixed parameter and therefore do not consider the influence of the heat transfer between the soil and the air circulating in the well on the temperature of the soil matrix [26–28]

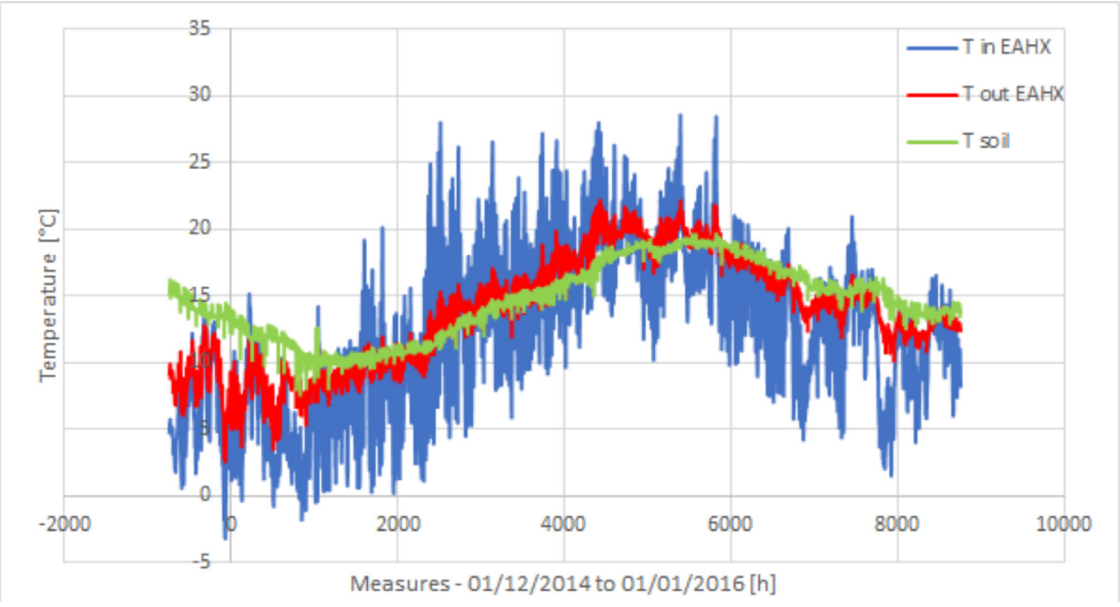

Fig. 2. Soil temperature measured at 2 m depth and EAHE inlet and outlet temperatures during the period from 01/12/2014 to 01/01/2016.

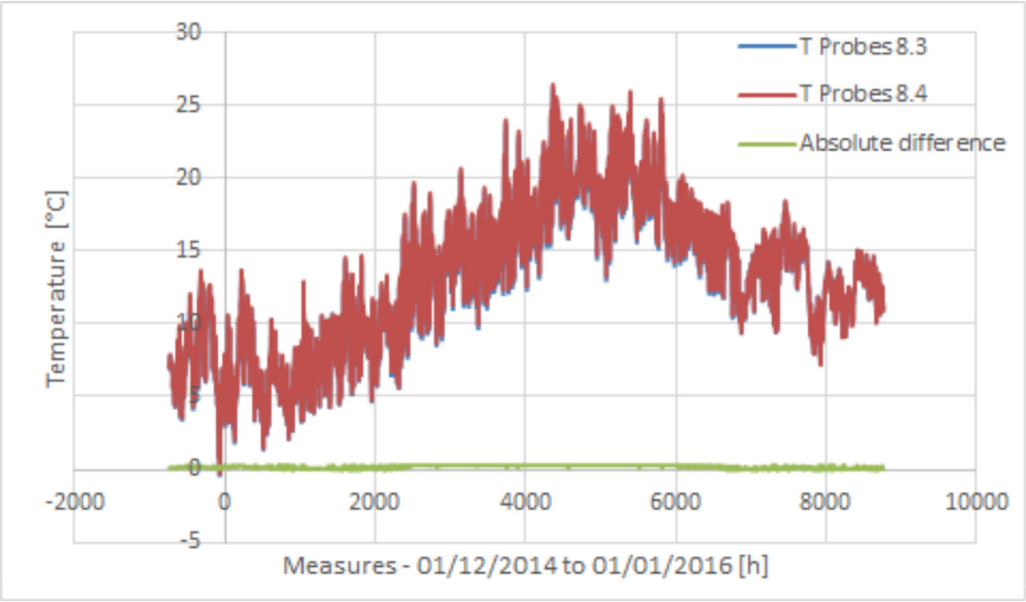

Fig. 3. Temperatures at the probes 8.3, 8.4 and absolute difference between these measures during the period from 01/12/2014 to 01/01/2016.

A more complex model has been developed by Pierre Hollmuller [29]. It's an in-depth analytical theoretical model validated by numerous in situ measurements to establish simple rules for the sizing of EAHE such as "the thumb rule". A sensitivity study on the physical characteristics of the soil and the heat transfer dynamics are analysed in the ideal case of a single tube buried in the ground. This model has been validated against a complete analytical solution as well as against two in-situ monitored systems with important latent heat transfers [30].

Pierre Tittelein [31] proposes a numerical model based on the COMSOL software that discretised the well in different parts. In each slice, a calculation of response factors is performed using COMSOL to reduce the calculation time. The proposed model is then compared to an analytical model. He showed that the flow of heat entering the tube is a function of the temperature of the air flowing through the pipe. To find the output temperature, a heat balance equation is applied. The problem encountered using the model mentioned above is that it took a long time to calculate the behaviour of the heat exchanger accurately due to the type of mesh required.

Other numerical models using finite element or finite difference consider the complete geometry of the problem in 2D [32] or in 3D [33]. Some models do not consider the fact that the entire soil is influenced by the exchanger [34]. Others solve a thermal balance at the surface of the ground and a model of exchanger with a single tube like [35].

Lee et al. [36] used the Energy Plus software and created a mathematical model. A detailed algorithm was used to calculate the evolution of the soil temperature for each pipe and for each time step. Thiers et al. [37] laid several tubes in parallel at the same depth. The finite volume method with a limited number of nodes was used. Two concentric cylindrical meshes were used for each tube to study the interaction between several parallel pipes laid at the same depth.

In our study, we propose three different models to study the EAHE: two 3D numerical models (complete and simplified) and a pseudo 3D model. The 3D models accurately consider the 3D heat diffusion inside the soil and at the level of the pipes, but only consider sensible heat transfers. The pseudo 3D model can also take into account the condensation phenomena.

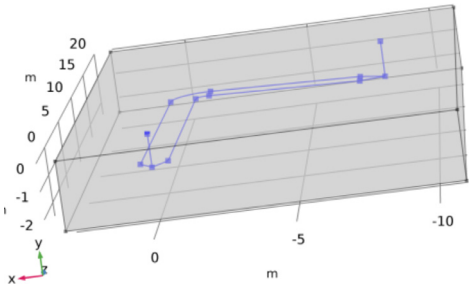

Fig. 4. Full-scale 3D model.

4.2. 3D numerical model

To model the heat transfer and fluid flow in our system, the 3D models use "physics" modules available in COMSOL software. The module "heat transfer in solids" to model the thermal behavior of soil and "heat transfer in pipe" for the EAHE modeling.

A complete model (Full-scale 3D model) and a simplified model (Simplified 3D model) were carried out in order to compare the results between them and with the experimental data to check the simplifying assumption applied to the simplified model. In this latter model, the vertical parts and bends are not considered.

The full-scale 3D model, represented on the Fig. 4, has a depth of 2.5 m, a width of 14 m and a length of 23 m. The simplified 3D model, represented on the Fig. 5, has a depth of 2.5 m, a width of 5.5 m and a length of 25 m.

4.2.1. Initial condition

The initial condition of the soil is set as follows, the temperature of the soil matrix was defined as being equal to the soil temperature at a depth of 1 m on December 1, 2014, date of the beginning of simulation. It is therefore 15.2 °C.

4.2.2. 3D models boundary conditions

The different boundary conditions of the 3D models are identified on Tables 2 and 3.

Table 2
Boundary conditions of the complete 3D model.

Boundary 1	*Boundary 2*	*Boundary 3*	*Boundary 5*
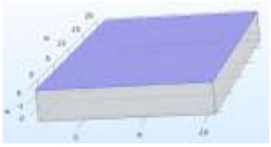	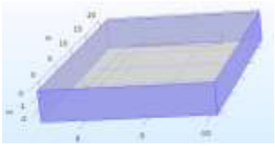	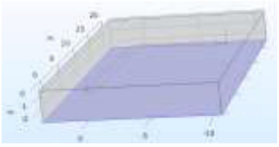	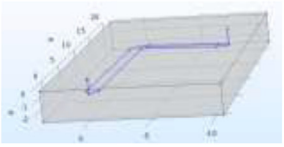

Table 3
Boundary conditions of the simplified 3D model.

Boundary 1	*Boundary 2*	*Boundary 3*	*Boundary 4*	*Boundary 5*
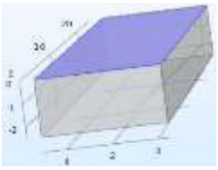	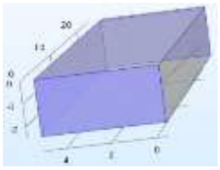	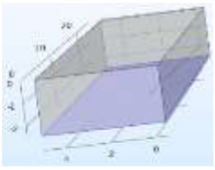	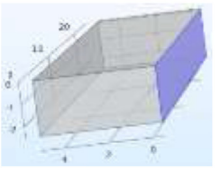	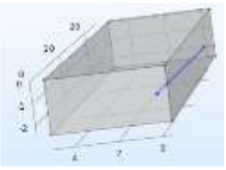

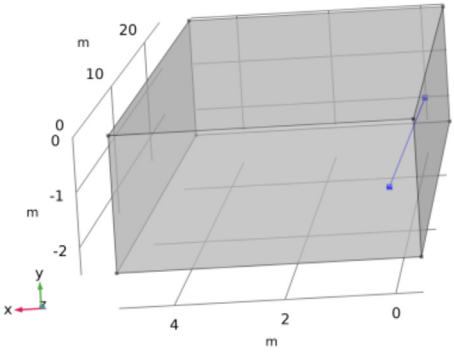

Fig. 5. Simplified 3D model.

Boundary 1 represents the interface between the ground and the external environment. The boundary condition is expressed in the form:

$$\vec{n} \cdot \left(k \cdot \vec{\nabla} T\right) = q_{solar} + h_{surface} \cdot (T_{ext} - T) + \varepsilon \cdot \sigma \cdot \left(T_{env}^4 - T^4\right) \quad (1)$$

To simplify the model, the temperature T_{env} is assimilated to the temperature $T_{ext.}$ Boundary 2 is considered to be adiabatic. Boundary 3 represents the water table, it is a Dirichlet condition. The imposed temperature has been defined as the arithmetic mean of the outside temperatures of 2015: 12.4 °C. Boundary 4 is the symmetry plane of the model and will therefore be considered adiabatic. Boundary 5 represents the inside of the tube, modelized by the physics "heat transfer in pipe" and which considers an internal film resistance characterized by a Nusselt number of 3.66 (calculation of the viscous boundary layer) for the circular sections and a conductive heat transfer within the material composing the pipe. The thickness of the pipe is 1 mm and its conductivity k is 0.49 $W.m^{-1}.K^{-1}$.

4.3. Pseudo 3D numerical model

In the pseudo 3D model, the EAHE is discretized over its length in different parts called sections (Fig. 6). The heat transfer between the soil and the interior air of the EAHE is considered uniform within the section and is calculated in the normal plane to the tube (2D inlet of the section).

Different phenomena take place within the soil: conduction, convection and radiation. For a simplified approach of the temperature field in the soil, a pure conductive model is acceptable. Indeed, the radiative transfer is rather weak considering the small temperature gradients. Evaporation and convection can also be neglected as demonstrated by a study on heat transfer in porous media [38]. After having analyzed both 3D models, we have checked that the vertical parts of the EAHE, with a large internal diameter of 375 mm, have a very limited impact on the global heat transfer. The vertical parts accounted for 4.8% of the global heat transfer the coldest day of the year, and for 1.1% the warmest day of the year. So, they have not been integrated in the pseudo 3D model.

The initial condition is identical to the one of the 3D models presented previously.

4.3.1. Boundary conditions of the pseudo 3D model

The different boundary conditions of the pseudo 3D model are identified on Fig. 7.

The boundary conditions of the pseudo 3D model are identical to those of the 3D models described in the 4.2.2 point except for the boundary 5. For this boundary, at first, only convective heat transfer has been considered. This corresponds to a Fourier condition (see algorithm on Fig. 8). In a second time, the phenomenon of condensation is taken into account and a Neumann condition will be added. The energy balance on the 5th boundary is then expressed as follows:

$$\vec{n} \cdot \left(k \cdot \vec{\nabla} T\right) = \underbrace{h_{tube} \cdot \frac{c_a}{c_H} \cdot (T_{air} - T_{wall})}_{Fourier\ condition} + \underbrace{q_0}_{Neumann\ condition} \quad (2)$$

T_{wall} is known at each node of the boundary and we take then an average value $T_{wall,m}$ to evaluate the mean heat transfer coefficient. Knowing the air temperature and its velocity, the mean wall temperature, we evaluate *Re*, Pr and Nu numbers to determine the convective heat transfer coefficient between the air located in the section and the inner wall of the pipe.

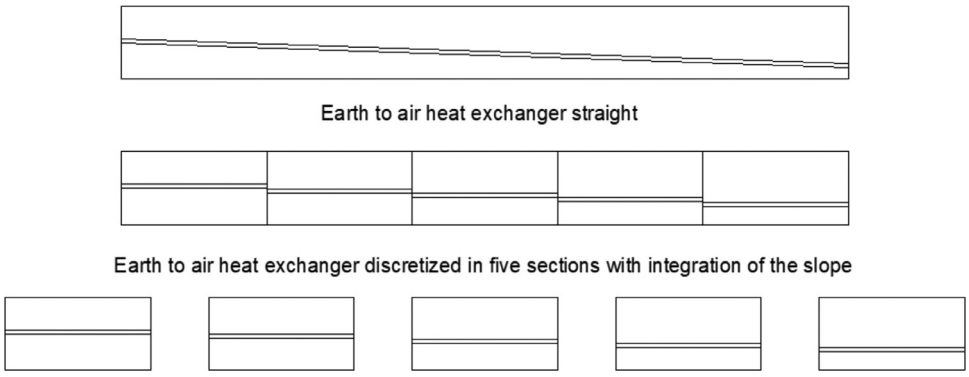

Fig. 6. Pseudo 3D modeling, discretization of the EAHE in different sections.

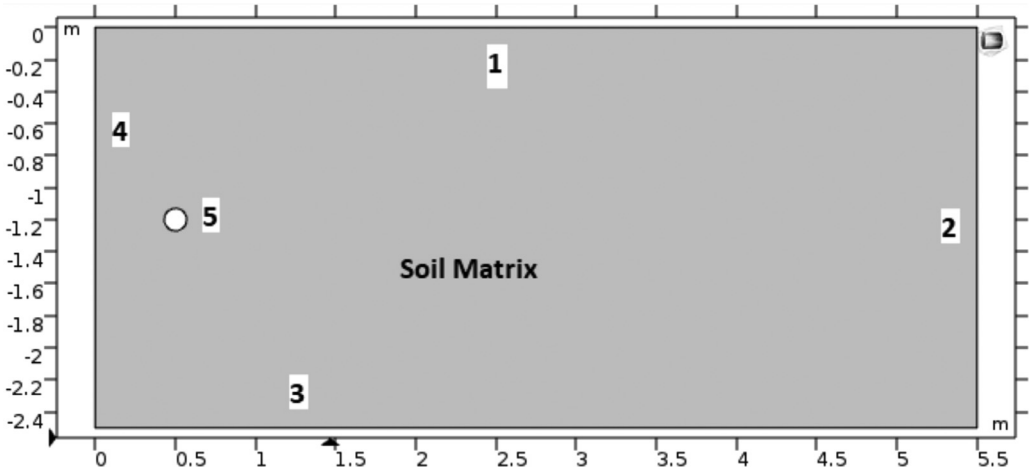

Fig. 7. Boundary conditions of the pseudo 3D model (2D inlet section).

f and Nu have been calculated with the Gnielinski's formula [39,40]:

$$f = (0,790 \cdot \ln Re - 1,64)^{-2} \quad for\ smooth\ tube \tag{3}$$

$$Nu = \frac{\frac{f}{8} \cdot (Re - 1000) \cdot Pr}{1 + 12,7 \cdot \left(\frac{f}{8}\right)^{\frac{1}{2}} \cdot \left(Pr^{\frac{2}{3}} - 1\right)} \quad for \begin{bmatrix} 0,5 < Pr < 2000 \\ 2300 < Re < 5.10^6 \end{bmatrix} \tag{4}$$

Prandtl and Reynolds numbers are respectively around 0.716 and 22.10^3 within the EAHE.

To determine if there is condensation, the humidity ratio x of the air entering the section is compared to the saturation humidity ratio x_{sat} for the temperature $T_{wall,m}$ at each time step. If x is higher than x_{sat}, there is condensation and q_0 must be determined. Fick's law applied to our case study, can be written:

$$M = K_D \cdot (Y_{air} - Y_{sat}) \tag{5}$$

Knowing that for an air-water mixture the Lewis number is considered equal to 1, we can establish that for the cooling of moist air in direct contact with a wall, the total flux is given as follows:

$$q_{tot} = \frac{h_{tube}}{c_H} \cdot \left(i_{air} - i_{sat}\left(T_{wall,\ m}\right)\right) \tag{6}$$

To determine the flux to be considered at the level of the 5th boundary, Eq. (6) has to be put in the form of Eq. (4). After resolution, we obtain:

$$q_0 = \frac{h_{tube}}{c_H} \cdot \left(c_v \cdot \left(x \cdot T_{air} - x_{sat}\left(T_{wall,m}\right) \cdot T_{wall,m}\right) + L_c \cdot \left(x - x_{sat}\left(T_{wall,\ m}\right)\right)\right) \tag{7}$$

4.3.2. Integration along the tube for the pseudo 3D model with condensation

This integration is done according to the algorithm illustrated in Fig. 8 and explained below. The algorithm used for heat transfer between dry air and soil is similar to the one developed by Elmer and Schiller [41]. Consideration of heat transfer due to condensation refers to the algorithm presented by Boulard et al. [42], validated by experimental data [33] and integrated in TRNSYS for multi-pipe systems [30].

The result of the 2D simulation (COMSOL without condensation) gives the average temperature at the wall surface of the tube for each hour. With this temperature $T_{wall,\ m}$ we can calculate the x_{sat} and compare this value to the humidity ratio x at the inlet of the section. For each time step, a flux is calculated according to Eq. (7) when there is condensation and taken equal to 0 when there is not. This heat flux is added to the fifth boundary of the COMSOL model and a new simulation allows us to determine the total heat flux Q_{tot} and a new temperature $T_{wall,\ m}$. On the entire section, the total heat flux is considered uniform between the internal surface of the pipe and the air circulating inside.

$$Q_{conv} = h_{tube} \cdot \left(T_{wall,m} - T_{air,in}\right).S_{section} \tag{8}$$

Knowing Q_{tot} and Q_{conv}, we can calculate Q_{lat} when there is condensation and the temperature and the absolute humidity at the end of the section, considering c_H as a constant along the section.

$$\begin{aligned} Q_{tot} &= Q_{conv} + Q_{lat} \\ &= \dot{m}_{air}.c_H\ \left(T_{air,out} - T_{air,in}\right) + \dot{m}_{air} \cdot L_c \cdot \left(x_{air,out} - x_{air,in}\right) \end{aligned} \tag{9}$$

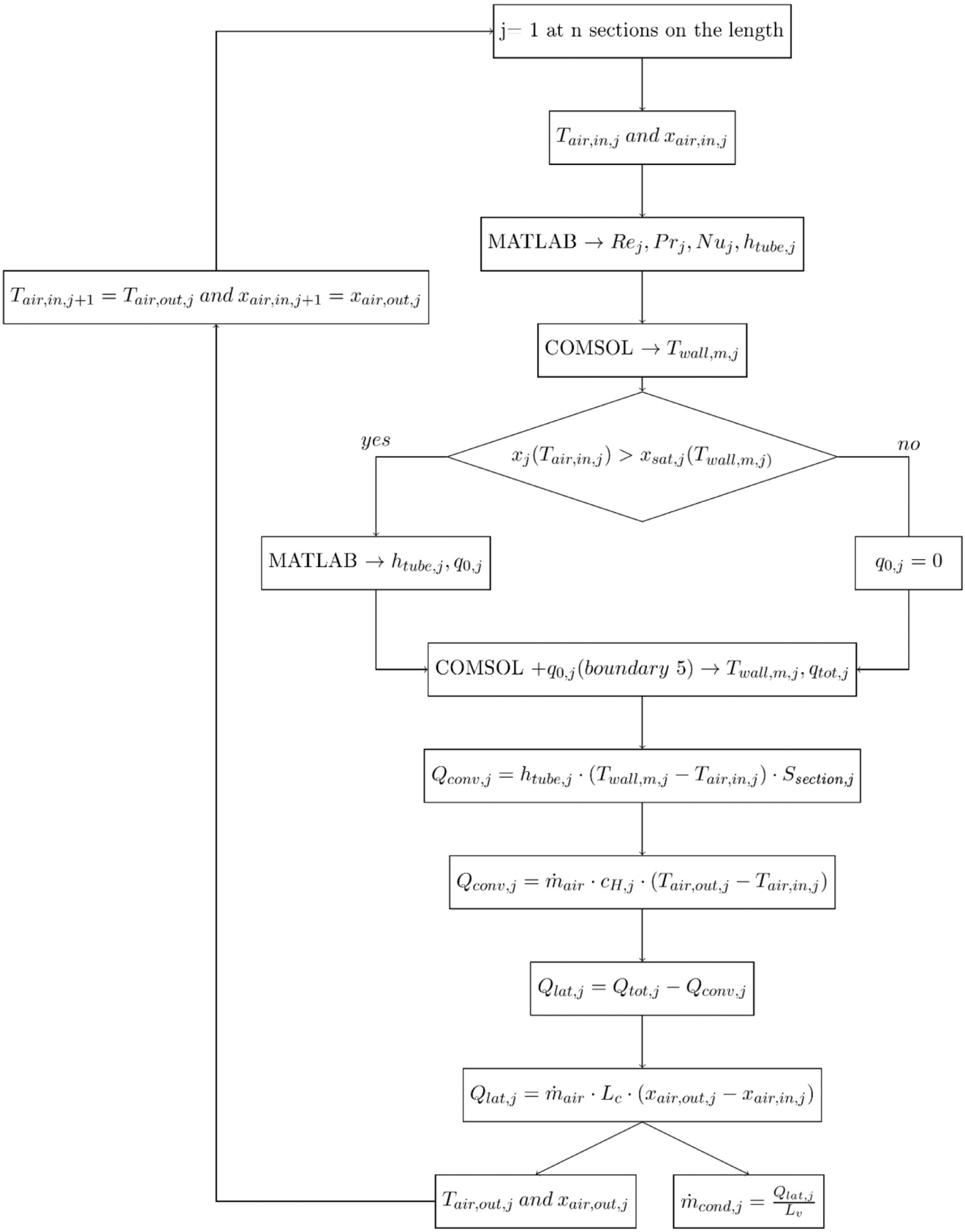

Fig. 8. Algorithm for solving the unsteady pseudo 3D problem considering condensation.

The temperature and the humidity ratio of the air at the exit of the considered section are then returned in the model as being the air temperature and the humidity ratio at the inlet of the next section.

The condensate flow produced is then calculated for the considered section to determine the total amount of condensate produced in the whole EAHE at each time step.

$$\dot{m}_{cond} = \frac{Q_{lat}}{L_c} \tag{10}$$

This model only considers condensation, but not evaporation. The pipes have a slope of 3% which allows condensates to accumulate in the bottom of the vertical pipe at the outlet of the EAHE. The free surface is relatively small, and the evaporation phenomenon is limited. Two to three times a year, the condensates are removed using an empty cellar pump installed for this purpose.

5. Sensitivity analysis, without condensation

To identify the parameters having an important influence on the results of the simulations, a series of sensitivity study was carried out, as defined in Sections 5.1–5.7. As the purpose of both 3D models – complete and simplified – is to validate the results obtained by the pseudo 3D model, the sensitivity study will mainly focus on the pseudo 3D model (but without condensation phenomena, which will be treated in Section 6). The results of the sensitivity analysis are summarized in Section 5.8 and given in all details is the Appendix.

In order to compare the accuracy of the different simulations, we calculated at the end of the pipe the temperature difference between the measured values and the simulated values for the whole year of 2015. We then calculated an average of the absolute values of the errors according to the formula:

$$e_a = \frac{\sum_{j=1}^{8760} \left| T_{\text{measured j}} - T_{\text{simulated j}} \right|}{8760} \tag{11}$$

$$e_{\max} = \max_{j=1}^{8760} \left| T_{\text{measured j}} - T_{\text{simulated j}} \right| \tag{12}$$

5.1. EAHE discretization

This parameter was only analyzed for the pseudo 3D model. Each horizontal part of the EAHE is 25 m long and the air flow conditions are identical in both pipes constituting the EAHE. Several numerical simulations were performed by discretizing the total length of the EAHE into different parts or segments: 1×25 m (only one segment), 5×5 m (5 segments), 10×2.5 m (10 segments) and 25×1 m (25 segments).

5.2. Slope of the EAHE

The depth of the "horizontal" parts of the EAHE is 1.2 m at the inlet and 1.95 m at the outlet, given the 3% gradient allowing the condensate flow. In the pseudo 3D model, this slope can be considered by giving each section of the EAHE its actual average depth. In the full-scale 3D model and the simplified 3D model, the slope is easily modelized.

5.3. Soil characteristics

The density of the soil could be measured and determined and therefore will not be modified. Regarding the thermal capacity and the thermal conductivity of the soil, they were chosen based on the usual values for the type of soil considered (see Table 1). However, due to the heterogeneous nature of the soil, different simulations have been carried out taking into account a heat capacity of 1000 or 900 $J.kg^{-1}.K^{-1}$ and a thermal conductivity of 0.58, 0.85 or 1 $Wm^{-1}.K^{-1}$ which may vary due to moisture [25].

5.4. Depth and temperature of the water table

The depth of the water table was estimated at 2.5 m based on a soil analysis report. Since the depth of the water table may vary over time, simulations for depths of 2.05 m, 2.5 m, 3 m, 4 m, 10 m and 50 m have been carried out.

The water table temperature is the third boundary of the numerical model as shown in Fig. 7. It was initially taken equal to the average annual outdoor temperature (12.4 °C). In a second time, this water table temperature has been considered as equal to the monitored soil temperature at 2 m depth (Fig. 2), i.e. variable over time. Finally, it was considered equal to the annual average of the monitored soil temperature (14.6 °C).

5.5. Convective heat transfer coefficient along the tube wall

This parameter was only analyzed for the pseudo 3D model. For the first simulations, this h_{tube} coefficient was considered constant and equal to 9.26 $W.m^{-2}.K^{-1}$, the value obtained for the average temperature of the year, 12.5 °C.

In a second step, this coefficient was considered as variable in the simulations and calculated at each time step and for each section according to the thermal and mechanical characteristics of the air according to formulas 3 and 4 at the boundary 5. Its value varies between 9.05 $W.m^{-2}.K^{-1}$ and 9.49 $W.m^{-2}.K^{-1}$.

5.6. Convective heat transfer coefficient at ground level

For the first simulations, $h_{surface}$ coefficient was considered constant and equal to 23 $W.m^{-2}.K^{-1}$. In a second step, the coefficient was considered as variable in the simulations and calculated at each time step according to the thermal characteristics of the air and the wind speed. To calculate this coefficient, two methods were used.

For the first method, the flow is considered as a longitudinal flow parallel to a plate of length d. The length was initially considered to be equal to 10 m to be modified after by varying the value of d in steps of 5 m from 10 m to 55 m.

The empirical formulas in [39] allowing the calculation of this convective heat transfer coefficient are:

$$Nu = 0,664 \cdot Re^{0,5} \cdot Pr^{\frac{1}{3}} \quad for\ Re < 4 \cdot 10^5 \tag{13}$$

$$Nu = 0,037 \cdot Re^{0,8} \cdot Pr^{\frac{1}{3}} \quad for\ Re \geq 4 \cdot 10^5 \tag{14}$$

The Reynolds number is calculated on the basis of the wind speed and the selected characteristic dimension d. The $h_{surface}$ values obtained for a d equal to 10 m are between 0 $W.m^{-2}.K^{-1}$ and 42.53 $W.m^{-2}.K^{-1}$, whereas for a d equal to 55 m, they vary between 0 $W.m^{-2}.K^{-1}$ and 30.24 $W.m^{-2}.K^{-1}$.

The second method is based on an empirical equation taken up from the works and articles [43,44] linking the $h_{surface}$ convective heat transfer coefficient and the wind speed. This equation is:

$$h_{surface} = 0,5 + 1,2 \cdot \sqrt{v_{wind}} \tag{15}$$

5.7. 2D model and 3D model meshes

In the pseudo 3D model, there is a 2D finite element mesh in the section of the EAHE. Several simulations were performed using different meshes to ensure the needed mesh independence of the

Table 4
Characteristics of the various studied meshes.

	Normal mesh 2D model	*Fine mesh 2D model*	*Very fine mesh 2D model*	*Mesh 3D simplified*
Mesh points	483	798	6727	414
Triangle elements	892	1484	13130	546
Edge elements	74	112	324	124
Point elements	8	8	8	10
Simulation's time	218 s	353 s	2657 s	1794 s
e_a – Absolute error	0,98 K	0,98 K	0,98 K	1,04 K
e_{max} – maximum error	3,19 K	3,19 K	3,19 K	3,50 K
Illustrations	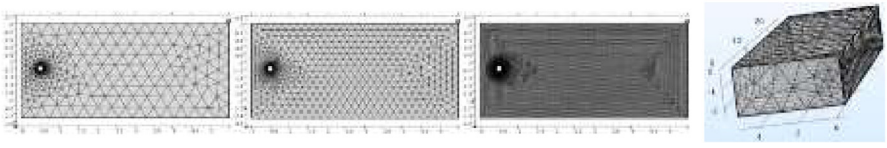			

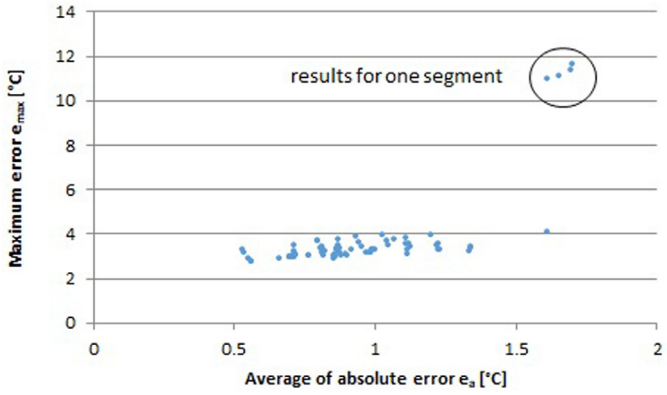

Fig. 9. Pseudo 3D model: maximum versus average error, for the different simulations.

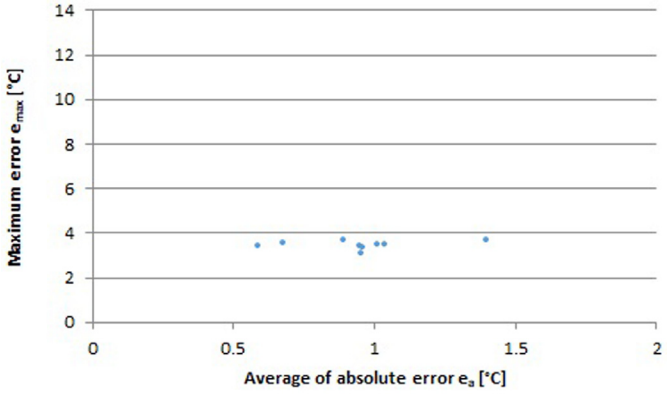

Fig. 10. 3D models: maximum versus average error, for the different simulations.

model. The COMSOL software allows a choice of semi-automatic mesh whose characteristics for a water table located at 2.5 m are shown in Table 4.

5.8. Results of the sensitivity study

The results of the sensitivity analysis are summarized in Fig. 9 (Pseudo 3D model) and 10 (3D models), in terms of maximum and average absolute hourly difference with the monitored data (see Eqs. (11) and (12)). Detailed simulation results by scenario can be found in the Appendix in Fig. 13 for the results of the pseudo 3D model and Fig. 14 for the results of the 3D models.

We can see on Fig. 9 that the numerical simulations make it possible to obtain interesting results. The set of simulations also tends to prove that the discretization of the EAHE, in the pseudo 3D model, in a large number of segments does not bring any improvement on the precision of the results. However, the comparison of the results with the simulations carried out for a single segment (equal to the total length of the EAHE - (Appendix, Fig. 13, simulation number 9, 15, 24 and 27)) puts forward the importance of discretization the length of the EAHE into several sections as shown in Fig. 9.

As can be seen in Fig. 10, the results obtained with the 3D models are quite close to the results of the pseudo 3D model and are not more accurate. The pseudo 3D model is therefore validated, and the condensation will be integrated into it.

Taking into account the slope of the EAHE would have a detrimental effect on the results, and this phenomenon could be related to the presence of the water table close to the EAHE. Indeed, the

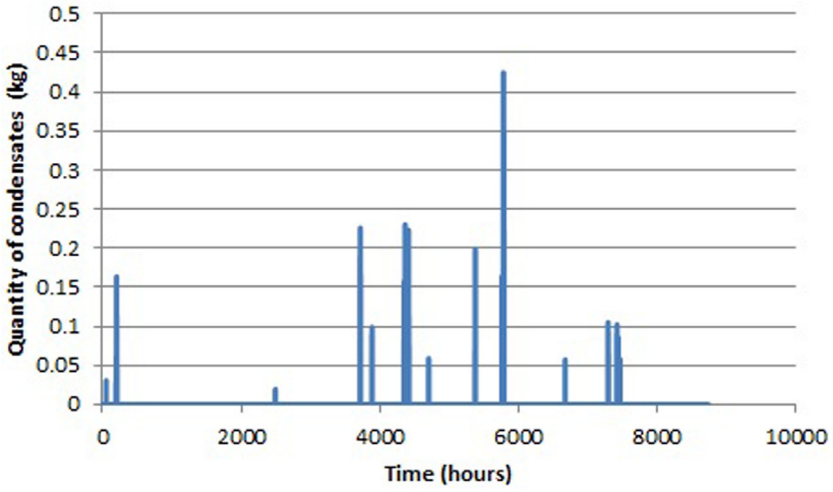

Fig. 11. Quantity of condensates produced in 2015 in one of the two tubes - results of the pseudo 3D model.

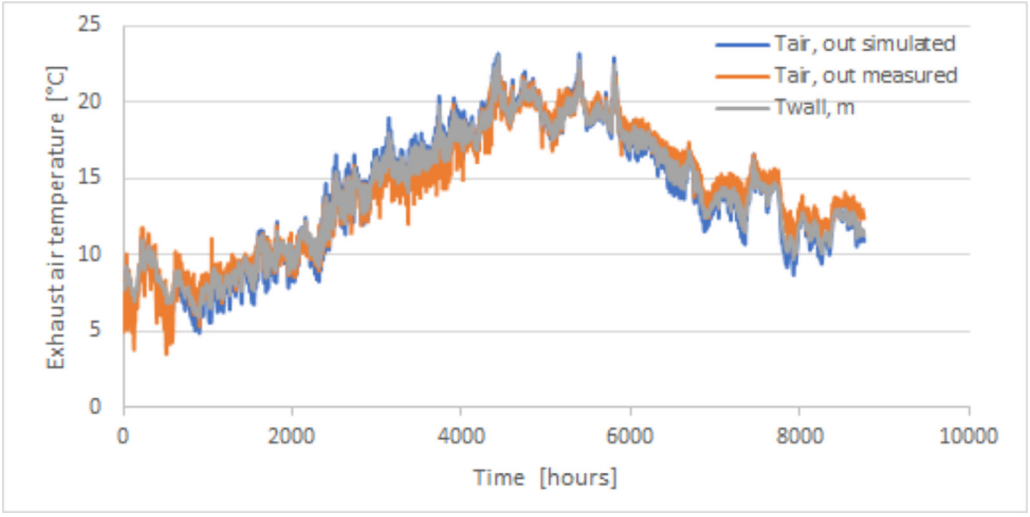

Fig. 12. Exhaust air temperatures measured and simulated and wall temperature at the outlet on the basis of the pseudo 3D model with condensation.

deeper the water table, the more the consideration of the slope of the EAHE in the simulations gives results close to the experimental readings compared to taking a constant EAHE depth. The average absolute error on temperature e_a decreases of 0.04 K for a water table depth of 2.5 m (Appendix, Fig. 13, comparing simulation numbers 10 and 65), decreases of 0.18 K to 0.15 K for a water table depth of 10 m (Appendix, Fig. 13, comparing simulation numbers 16 and 19, 17 and 20, 18 and 21) and decreases of 0.16 K for a water table depth of 50 m (Appendix, Fig. 13, comparing simulation numbers 22 and 23).

The so-called "Normal" mesh (see Table 4) makes it possible to obtain sufficiently precise results and it is thus not necessary to choose finer meshes unnecessarily increasing the computation time.

Besides this general result, we would like to point out following specific issues:

- Physical properties of the soil:
  - They have an impact on the results of the simulations. For discretization in 10 or 25 segments, when the conductivity changes from 0.58 to 0.85 $W.m^{-1}.K^{-1}$, the results are more accurate of 0.11 K compared to the experimental data if the depth variation of the EAHE is taken into account (Appendix, Fig. 13, comparing simulation numbers 13 and 54, 14 and 55). In the case of a fixed depth of 1.2 m, its impact is very small about of 0.01 K (Appendix, Fig. 13, comparing simulation numbers 10 and 50, 11 and 51). Taking a heat capacity of 900 instead of 1000 $J.kg-^{1}.K^{-1}$, or changing the heat conductivity from 0.85 to 1 $W.m^{-1}.K^{-1}$, does not influence significantly the results of the simulations especially if the depth variation of the EAHE is taken into account, no more of 0.02 K (Appendix, Fig. 13, comparing simulation numbers 48 and 54, 49 and 55, 53 and 59, 54 and 60, 55 and 61).
- Convective heat transfer at ground level:
  - The second method for calculating $h_{surface}$ gives results of simulations higher than 0.44 K in ea compared to the results obtained with the first method of calculation and a reference length d of 10 m (Appendix, Fig. 13, simulation number 62 and 65).
  - By increasing the distance d from 10 m to 55 m, the $h_{surface}$ will be increased and the results of the simulations will be

Table 5
Average absolute and maximum errors for the different simulations compared to the experimental data.

	3D Simplified	Full-scale 3D model	Pseudo 3D without condensation	Pseudo 3D with condensation
e_a	0.95	0.92	0.70	0.72
e_{max}	3.46	3.17	2.95	2.98

improved in the order of 0.07 K in EA (Appendix, Fig. 13, simulation number 65 at 73).

- Convective heat transfer inside the EAHE
  - The choice to compute the h_{tube} for each time step and for each section does not really influence the results of the simulations compared to a fixed value of 9.26 $W.m^{-2}.K^{-1}$ (Appendix, Fig. 13, simulation number 25 at 45).

6. Numerical simulation, with/without condensation

The parametric study concluded that the optimum non-condensing pseudo 3D model was a EAHE discretized in five segments whose slope is taken into account and for which the depth of each section will be different. ρ is 1800 $kg.m^{-3}$, c is 1000 $J.kg^{-1}.K^{-1}$ and k is equal to 0.58 $W.m^{-1}.K^{-1}$. The depth of the water table being variable throughout the year, a depth of 2.5 m was considered. The convective heat transfer coefficients along the tube and soil surface were considered variable and calculated for each time step and each section. The convective heat transfer coefficient at the soil surface was calculated with a flow considered to be longitudinal and parallel to a plate of length d equal to 55 m. The mesh was chosen semi-automatically and defined by the software as “Normal”. The simulation results for the different models studied are shown in Table 5.

With those results we can confirm the simplifying assumptions made on the simplified 3D model and pseudo 3D models. Taking into account condensation does not significantly impact the results of the simulations. This is due to the small amounts of condensate produced during the year as shown on Fig. 11.

A phenomenon currently studied [45,46] could explain the differences between measured and simulated values. Indeed, the physical characteristics of the soil are considered constant throughout the year, while its humidity varies over time and modifies its physical characteristics.

The total amount of condensate produced in the EAHE (2 tubes) during the year 2015 is 25.22 kg (result of the simulation of the pseudo-3D model). It is during June, July and August that most of the condensation takes place. Outside this period, we note a low condensate production taking place around the 10/01/2015. This is due to outside temperatures above seasonal normals and a relatively high relative humidity.

The average of the temperatures of the inner surface of the last segment of the pipe $T_{wall,m,n}$ is quite close to the temperature of the condensates produced, so we can see that these condensates will have temperatures between 6 °C and 23 °C, illustrated on Fig. 12. These temperatures are very conducive to the development of psychrophilic microorganisms.

7. Conclusion and future work

After a state of the art on the EAHE technique, we presented the installation studied and the monitoring system as well as the results obtained. We then developed different models of EAHE: complete 3D model, simplified 3D and pseudo 3D after a study of the models encountered in the literature. To identify the parameters having a significant influence on the results of the simulations, a sensitivity study was carried out. We have finally been able to model the condensation phenomenon and to characterize the condensates obtained using the pseudo 3D model.

We can conclude that the difference between the results of the simulations and the measurement is quite small. A conclusive numerical model has been developed and can serve as a basis for further studies although some parameters may still require further analysis.

The pseudo 3D model could be improved by taking into account the evaporation phenomenon. This occurs partly in the pipes but mainly in the bottom of the vertical outlet pipe where condensate accumulates. An analysis of the thermal conductivity of the soil should also be carried out because this value has a significant impact on the results.

In the particular case of our experimental setting, simulation shows that the geometry of the EAHE favors the generation of condensate. These cannot be evacuated with a drain to avoid air contamination by radon. They are partly eliminated using an empty cellar pump two to three times a year. The produced condensate is too small to impact the temperature at the well outlet. However, should it remain within the pipes or the vertical outlet shaft for sufficient time before evaporating again, it might allow the development of microorganisms that could contaminate hygienic air. As a complement to simulation, monitoring of inlet and outlet air humidity would be a straightforward way to compute an hourly water balance concerning condensation, evaporation and stagnant water.

The pseudo 3D model will be used as a basis for characterization of the biotope. We intend to study the biocenosis by carrying out experimental surveys in order to know the different species present by means of microscopic analyzes, cultivations and metagenomic analyzes. As the microorganisms are identified, we will be able to estimate whether there is a health risk by comparing the growth conditions of pathogenic microorganisms with the biotope characteristics obtained using our numerical model.

Declaration of Competing Interest

We wish to confirm that there are no known conflicts of interest associated with this publication and there has been no significant financial support for this work that could have influenced its outcome.

Supplementary material

Supplementary material associated with this article can be found, in the online version, at doi:10.1016/j.enbuild.2019.109532.

Appendix

Figs. 13 and 14.

Simulation number	Segments	Slope	c	k	Depth of water table	Temperature of water table	h_{tube}	$h_{surface}$	mesh	e_a	e_{max}
			$J.kg^{-1}.K^{-1}$	$W.m^{-1}.K^{-1}$	m	°C	$W.m^{-2}.K^{-1}$	$W.m^{-2}.K^{-1}$		K	K
1	5	no	1000	0.58	2.5	12.4	Variable	Variable - d=10m	very fine	0.8	3.68
2	10	no	1000	0.58	2.5	12.4	Variable	Variable - d=10m	very fine	0.81	3.4
3	25	no	1000	0.58	2.5	12.4	Variable	Variable - d=10m	very fine	0.82	3.24
4	10	yes	1000	0.58	2.5	12.4	Variable	Variable - d=10m	very fine	0.98	3.19
5	25	yes	1000	0.58	2.5	12.4	Variable	Variable - d=10m	very fine	0.99	3.29
6	25	no	1000	0.58	2.5	12.4	Variable	Variable - d=10m	fine	0.82	3.24
7	10	yes	1000	0.58	2.5	12.4	Variable	Variable - d=10m	fine	0.98	3.19
8	25	yes	1000	0.58	2.5	12.4	Variable	Variable - d=10m	fine	0.99	3.29
9	1	/	1000	0.58	2.5	12.4	Variable	Variable - d=10m	normal	1.61	10.97
10	5	no	1000	0.58	2.5	12.4	Variable	Variable - d=10m	normal	0.8	3.67
11	10	no	1000	0.58	2.5	12.4	Variable	Variable - d=10m	normal	0.81	3.39
12	25	no	1000	0.58	2.5	12.4	Variable	Variable - d=10m	normal	0.82	3.24
13	10	yes	1000	0.58	2.5	12.4	Variable	Variable - d=10m	normal	0.98	3.19
14	25	yes	1000	0.58	2.5	12.4	Variable	Variable - d=10m	normal	0.99	3.29
15	1	/	1000	0.58	10	12.4	Variable	Variable - d=10m	normal	1.65	11.09
16	5	no	1000	0.58	10	12.4	Variable	Variable - d=10m	normal	0.71	3.52
17	10	no	1000	0.58	10	12.4	Variable	Variable - d=10m	normal	0.71	3.24
18	25	no	1000	0.58	10	12.4	Variable	Variable - d=10m	normal	0.71	3.08
19	5	yes	1000	0.58	10	12.4	Variable	Variable - d=10m	normal	0.53	3.18
20	10	yes	1000	0.58	10	12.4	Variable	Variable - d=10m	normal	0.55	2.91
21	25	yes	1000	0.58	10	12.4	Variable	Variable - d=10m	normal	0.56	2.76
22	25	no	1000	0.58	50	12.4	Variable	Variable - d=10m	normal	0.72	3.09
23	25	yes	1000	0.58	50	12.4	Variable	Variable - d=10m	normal	0.56	2.76
24	1	/	1000	0.58	2.5	12.4	Variable	23	normal	1.7	11.62
25	5	no	1000	0.58	2.05	12.4	9.26	23	normal	1.22	3.5
26	10	yes	1000	0.58	2.05	12.4	9.26	23	normal	1.61	4.12
27	1	/	1000	0.58	2.5	12.4	9.26	23	normal	1.69	11.36
28	5	no	1000	0.58	2.5	12.4	9.26	23	normal	1.11	3.85
29	10	no	1000	0.58	2.5	12.4	9.26	23	normal	1.12	3.57
30	25	no	1000	0.58	2.5	12.4	9.26	23	normal	1.13	3.42
31	5	yes	1000	0.58	2.5	12.4	9.26	23	normal	1.34	3.24
32	10	yes	1000	0.58	2.5	12.4	9.26	23	normal	1.34	3.36
33	25	yes	1000	0.58	2.5	12.4	9.26	23	normal	1.34	3.46
34	5	no	1000	0.58	3	12.4	9.26	23	normal	1.03	3.96
35	10	no	1000	0.58	3	12.4	9.26	23	normal	1.04	3.68
36	25	no	1000	0.58	3	12.4	9.26	23	normal	1.05	3.52
37	5	yes	1000	0.58	3	12.4	9.26	23	normal	1.22	3.55
38	10	yes	1000	0.58	3	12.4	9.26	23	normal	1.23	3.27
39	25	yes	1000	0.58	3	12.4	9.26	23	normal	1.23	3.29
40	5	no	1000	0.58	4	12.4	9.26	23	normal	0.93	3.89
41	10	no	1000	0.58	4	12.4	9.26	23	normal	0.94	3.6
42	25	no	1000	0.58	4	12.4	9.26	23	normal	0.95	3.45
43	5	yes	1000	0.58	4	12.4	9.26	23	normal	1.11	3.56
44	10	yes	1000	0.58	4	12.4	9.26	23	normal	1.11	3.27
45	25	yes	1000	0.58	4	12.4	9.26	23	normal	1.12	3.12
46	10	no	900	0.85	2.5	12.4	Variable	Variable - d=10m	normal	0.86	3.12
47	25	no	900	0.85	2.5	12.4	Variable	Variable - d=10m	normal	0.86	2.97
48	10	yes	900	0.85	2.5	12.4	Variable	Variable - d=10m	normal	0.89	3.12
49	25	yes	900	0.85	2.5	12.4	Variable	Variable - d=10m	normal	0.9	3.00
50	5	no	1000	0.85	2.5	12.4	Variable	Variable - d=10m	normal	0.81	3.41
51	10	no	1000	0.85	2.5	12.4	Variable	Variable - d=10m	normal	0.81	3.15
52	25	no	1000	0.85	2.5	12.4	Variable	Variable - d=10m	normal	0.82	3.01
53	5	yes	1000	0.85	2.5	12.4	Variable	Variable - d=10m	normal	0.86	3.39
54	10	yes	1000	0.85	2.5	12.4	Variable	Variable - d=10m	normal	0.87	3.17
55	25	yes	1000	0.85	2.5	12.4	Variable	Variable - d=10m	normal	0.88	3.05
56	5	no	1000	1	2.5	12.4	Variable	Variable - d=10m	normal	0.86	3.27
57	10	no	1000	1	2.5	12.4	Variable	Variable - d=10m	normal	0.85	3.04
58	25	no	1000	1	2.5	12.4	Variable	Variable - d=10m	normal	0.85	2.92
59	5	yes	1000	1	2.5	12.4	Variable	Variable - d=10m	normal	0.87	3.75
60	10	yes	1000	1	2.5	12.4	Variable	Variable - d=10m	normal	0.87	3.51
61	25	yes	1000	1	2.5	12.4	Variable	Variable - d=10m	normal	0.88	3.37
62	5	yes	1000	0.58	2.5	12.4	Variable	Variable - v_{wind}	normal	1.2	3.95
63	5	yes	1000	0.85	3	12.4	Variable	Variable - d=25m	normal	0.92	3.28
64	5	yes	1000	0.85	3	12.4	Variable	Variable - d=40m	normal	1.00	3.3
65	5	yes	1000	0.58	2.5	12.4	Variable	Variable - d=10m	normal	0.76	3.04
66	5	yes	1000	0.58	2.5	12.4	Variable	Variable - d=20m	normal	0.72	3.01
67	5	yes	1000	0.58	2.5	12.4	Variable	Variable - d=25m	normal	0.71	2.99
68	5	yes	1000	0.58	2.5	12.4	Variable	Variable - d=30m	normal	0.71	2.98
69	5	yes	1000	0.58	2.5	12.4	Variable	Variable - d=35m	normal	0.7	2.97
70	5	yes	1000	0.58	2.5	12.4	Variable	Variable - d=40m	normal	0.7	2.97
71	5	yes	1000	0.58	2.5	12.4	Variable	Variable - d=45m	normal	0.7	2.96
72	5	yes	1000	0.58	2.5	12.4	Variable	Variable - d=50m	normal	0.7	2.95
73	5	yes	1000	0.58	2.5	12.4	Variable	Variable - d=55m	normal	0.7	2.95
74	5	yes	1000	0.58	2.5	14.6	Variable	Variable - d=10m	normal	0.66	2.9
75	5	yes	1000	0.58	2.05	14.6	Variable	Variable - d=10m	normal	1.07	3.73

Fig. 13. Pseudo 3D model: Results of the sensitivity study.

Simulation number	model	Slope	c	k	Depth of water table	Temperature of water table	h_{tube}	$h_{surface}$	mesh	e_a	e_{max}
			$J.kg^{-1}.K^{-1}$	$W.m^{-1}.K^{-1}$	m	°C	$W.m^{-2}.K^{-1}$	$W.m^{-2}.K^{-1}$		K	K
1	simplified	yes	1000	0.58	2.05	12.4	Variable	Variable - d=10m	normal	1.39	3.67
2	simplified	yes	1000	0.58	2.5	12.4	Variable	Variable - d=10m	normal	1.04	3.50
3	simplified	yes	1000	0.58	3	12.4	Variable	Variable - d=10m	normal	0.89	3.67
4	simplified	yes	1000	0.58	5	12.4	Variable	Variable - d=10m	normal	0.68	3.56
5	simplified	yes	1000	0.58	10	12.4	Variable	Variable - d=10m	normal	0.59	3.46
6	simplified	yes	1000	0.85	2.5	12.4	Variable	Variable - d=10m	normal	0.95	3.11
7	simplified	yes	1000	1	2.5	12.4	Variable	Variable - d=10m	normal	0.96	3.37
8	simplified	yes	1000	0.58	2.5	12.4	Variable	Variable - d=25m	normal	1.01	3.51
9	simplified	yes	1000	0.58	2.5	12.4	Variable	Variable - d=50m	normal	0.95	3.46
10	Full-scale	yes	1000	0.58	2.5	12.4	Variable	Variable - d=55m	fine	0.94	3.30
11	Full-scale	yes	1000	0.58	2.5	12.4	Variable	Variable - d=55m	normal	0.92	3.17

Fig. 14. 3D models: Results of the sensitivity study.

References

[1] D.Y. Goswami, S. Ileslamlou, Performance analysis of a closed loop climate control system using underground air tunnel, J. Sol. Energy Eng. 112 (1990) 76–81.
[2] T. Kusuda, P.R. Achenbach, Earth temperature and thermal diffusivity at selected stations in United States, ASHRAE Trans. 71 (1965).
[3] G. Mihalakakou, M. Santamouris, D. Asimakopoulos, Modelling the earth temperature using multiyear measurements, Energy Build. 19 (1992) 1–9.
[4] G. Mihalakakou, On the application of the energy balance equation to predict ground temperature profiles, Solar Energy 60 (1997) 181–190.
[5] M. Santamouris, Passive cooling dissipation techniques for buildings and other structures: the state of the art, Energy Build. 57 (2013) 74–94.
[6] L. Ozgener, A review on the experimental and analytical analysis of earth to air heat exchanger (eahe) systems in turkey, Renew. Sustain. Energy Rev. 15 (2011) 4483–4490.
[7] M.S. Hatamipour, A. Abedi, Passive cooling systems in buildings: some useful experiences from ancient architecture for natural cooling in a hot and humid region, Energy Convers. Manag. 49 (2008) 2317–2323.
[8] F. Jomehzadeh, A review on windcatcher for passive cooling and natural ventilation in buildings, part 1: indoor air quality and thermal comfort assessment, Renew. Sustain. Energy Rev. 70 (2017) 736–756.
[9] S. Déoux, Mission D'évaluation Sanitaire du Puits Canadien - Siège Social du Groupe Millet. Scientific report « Analyse Qualité Santé AQS® », Medieco, 2011.
[10] M. Barbat, Nettoyabilité des Puits Climatiques, 2012 Scientific Report, Costic.
[11] W. Fisk, How IEQ affects health, productivity, ASHRAE J. 44 (2002) 56–60.
[12] P. Wargocki, Productivity and health effects of high indoor air quality, in: Encyclopedia of Environmental Health, Elsevier, 2011, pp. 688–693.
[13] AFCN Agence fédérale de Contrôle Nucléaire, Le radon. Scientific Report. Belgique, 2007.
[14] D.G. Leo Samuel, Cooling performance and indoor air quality characteristics of an earth air tunnel cooled building, J. Metrol. Soc. India MAPAN 33 (2017) 147–158.
[15] B. Flückiger, H.U. Wanner, P. Lüthy, Mikrobielle Untersuchungen von Luftansaug-Erdregistern, ETHZ, 1997 Scientific report.
[16] C. Peretti, A. Zarrella, M. De Carli, R. Zecchin, The design and environmental evaluation of earth-to-air heat exchangers (EAHE). A literature review, Renew. Sustain. Energy Rev. 28 (2013) 107–116.
[17] R. Singh, R.L. Sawhney, I.J. Lazarus, V.V.N. Kishore, Recent advancements in earth air tunnel heat exchanger (EATHE) system for indoor thermal comfort application: a review, Renew. Sustain. Energy Rev. 82 (2018) 2162–2185.
[18] P. Hollmuller, B. Lachal, Air-soil heat exchangers for heating and cooling of buildings : design guidelines, potentials and constraints, system integration and global energy balance, Appl Energy 119 (2014) 476–487.
[19] S.K. Soni, M. Pandey, V. Nath Bartaria, Ground coupled heat exchangers: a review and applications, Renew. Sustain. Energy Rev. 47 (2015) 83–92.
[20] M. Kaushal, Geothermal cooling/heating using ground heat exchanger for various experimental and analytical studies: comprehensive review, Energy Build. 139 (2017) 634–652.
[21] N. Bordoloi, A. Sharma, H. Nautiyal, V. Goel, An intense review on the latest advancements of earth air heat exchangers, Renew. Sustain. Energy Rev. 89 (2018) 261–280.
[22] K.K. Agrawal, G. Das Agrawal, R. Misra, M. Bhardwaj, D.K. Jamuwa, A review on effect of geometrical, flow and soil properties on the performance of earth air tunnel heat exchanger, Energy Build. 176 (2018) 120–138.
[23] T.S. Bisoniya, A. Kumar, P. Baredar, Experimental and analytical studies of earth–air heat exchanger (EAHE) systems in India: a review, Renew. Sustain. Energy Rev. 19 (2013) 238–246.
[24] bcrcinisma. Mons, Reconstruction du Pertuis du Trouillon Entre la rue Valenciennoise et L'avenue Maistriaux. Campagne géotechnique, 2011 Technical report, Inisma, 19 décembre.
[25] D. Pahud, in: Geothermal Energy and Heat Storage, SUPSI – DCT – LEEE, Dipartimento Costruzioni e Territorio, Scuola Universitaria Professionale della Svizzera Italiana, 2002, p. 30.
[26] M. De Paepe, A. Janssens, Thermo-hydraulic design of earth-air heat exchangers, Energy Build. 35 (2003) 389–397.
[27] V. Badescu, B. Sicre, Renewable energy for passive house heating: II. Model, Energy Build. 35 (2003) 1085–1096.
[28] M.K. Ghosal, G.N. Tiwari, Modeling and parametric studies for thermal performance of an earth to air heat exchanger integrated with a greenhouse, Energy Convers. Manag. 47 (2006) 1779–1798.
[29] P. Hollmuller, Analytical characterisation of amplitude-dampening and phase-shifting in air/soil heat-exchangers, Int. J. Heat Mass Transf. 46 (2003) 4303–4317.
[30] P. Hollmuller, B.M. Lachal, Buried pipe systems with sensible and latent heat exchanges: validation of numerical simulation against analytical solution and long-term monitoring, in: International Building Performance Simulation Association (IBPSA – Montreal Canada), 2005, pp. 411–418.
[31] P. Tittelein, Étude des échangeurs air-sol par la méthode convolutive des facteurs de réponse, Conférence IBPSA France, 2008.
[32] M. Bojic, N. Trifunovic, G. Papadakis, S. Kyritsis, Numerical simulation, technical and economic evaluation of air-to-earth heat exchanger coupled to a building, Energy 22 (1997) 1151–1158.
[33] T. Boulard, E. Rajafinjohany, A. Baille, Heat and water vapour transfer in a greenhouse with an underground heat storage system part-II experimental result, Agric. Forest Meteorol. 45 (1989) 185–194.
[34] R. Kumar, S. Ramesh, S.C. Kaushik, Performance evaluation and energy conservation potential of earth–air–tunnel system coupled with non-air-conditioned building, Build. Environ. 38 (2003) 807–813.
[35] V. Badescu, Simple and accurate model for the ground heat exchanger of a passive house, Renew. Energy 32 (2007) 845–855.
[36] K.H. Lee, R.K. Strand, The cooling and heating potential of an earth tube system in buildings, Energy Build. 40 (2008) 486–494.
[37] S. Thiers, B. Peuportier, Thermal and environmental assessment of a passive building equipped with an earth-to-air heat exchanger in France, Solar Energy 82 (2008) 820–831.
[38] P. Burton, Analyse et Simulation Numérique des Performances du Stockage Géothermique de L'énergie Solaire Pour Chauffer des Bâtiments Master's thesis, Faculté Polytechnique de Mons, Private communication, 2006.
[39] A.F. Mills, in: Heat Transfer, McGraw-Hill Inc., US, 1992, p. 270.
[40] V. Gnielinski. Neue Gleichungen für den Wärmeund den Stoffübergang in Turbulent Durchströmten Rohren und Kanälen. Technical report, Forschung im Ingenieur-Wesen, 1975.
[41] D. Elmer, G. Schiller, A preliminary examination of the dehumidification potential of earth/air heat exchangers, in: Proceedings of the International Passive Cooling Conference, 1981, pp. 161–165. Miami, Florida.
[42] T. Boulard, E. Rajafinjohany, A. Baille, Heat and water vapour transfer in a greenhouse with an underground heat storage system part-I experimental results, Agric. Forest Meteorol. 45 (1989) 175–184.
[43] S. Thiers, Modélisation Thermique d'un Échangeur Air-Sol Pour le Rafraichissement de Bâtiments, Journée thématique SFT – IBPSA, 2007 Technical Report.
[44] B. Givoni, M. Mostrel, Windscreens in radiant cooling, Passive Solar J. 1 (1982) 229.
[45] J. Lopez, S. Decker, S. Ginestet, Projet Effipuits, performance énergétique de puits Canadien : impact du retour d'expérience sur les données d'entrée de la simulation, Conference AUGC-IBPSA, Congress act, 2012.
[46] S. Ginestet, J. Lopez, S. Decker, Energy Performance of Earth-Air Heat Exchanger: Impact of Various Input Parameters on Simulation Results, 13th Conference IBPSA, 2013.